RADIO SCIENCE Journal of Research NBS/USNC-URSI
Vol. 68D, No. 10, October 1964

Broadband Radio-Star Scintillations, II. Interpretation

D. G. Singleton [1]

Contribution From the High Altitude Observatory, Boulder, Colo.

(Received March 3, 1964; revised May 8, 1964)

The focusing action of horizontal elongated irregularities of electron density in the ionosphere is considered. Expressions are developed for the general case where the azimuths of the radio star and of the short dimension of the irregularity may each be different from the azimuth of the interferometer baseline. These expressions appear to explain the main features of broadband radiostar scintillations, namely (a) their bandwidth, (b) their position-shift patterns, and (c) the nature of their association with spread-F. To reconcile the theory with the occurrence data on scintillations which exhibit position shifts, it is necessary to postulate an irregularity movement towards an azimuth of 120°, i.e., a movement along the isoclines.

1. Introduction

Part I of this series [Singleton, 1964] discussed observations of Cassiopeia A made with the Boulder swept-frequency interferometer which operates in the frequency range 7.6 to 41 Mc/s. The scintillations observed were found to be broadband, to involve occasionally position shifts and dispersion and to be associated closely with spread-F. The aim of this part is to investigate to what extent refractive properties of ionospheric irregularities can be invoked to explain these observations.

2. Model Employed to Interpret Position Shifts

The broadband nature of the scintillations first observed by Wild and Roberts [1956] in the frequency range 40 to 70 Mc/s led them to postulate that the ionospheric irregularities responsible behaved as lenses. They assumed that the irregularities were physically larger than the first Fresnel zone and that as a consequence the deviations produced in an incoming plane wave front were due mainly to refraction rather than diffraction. In other words, the ionospheric lenses were considered to focus the energy of the radio star so as to produce simultaneous increases of intensity over a large range of wavelengths. Warwick [1964], working in the frequency range 7.6 to 41 Mc/s, has recently shown that such a focusing mechanism is consistent, not only with the broadband nature of the scintillations, but also with the configuration of position shifts which are occasionally associated with scintillations in this frequency range.

[1] On sabbatical leave from the Physics Department, University of Queensland, Australia.

Warwick's analysis involved the rather special case in which the line-of-sight to the source, the interferometer baseline and the short dimension of the focusing irregularity (assumed elongated and horizontal) are taken as coplanar. Here an analysis is outlined which is similar to Warwick's but which deals with the general case where the azimuth of the source and that of the short dimension of the irregularity may each be different from the azimuth of the interferometer baseline. In the first instance a flat earth approximation will be discussed for elongated horizontal irregularities. The effect on the results of changing to a spherical earth and ionosphere and allowing the irregularities to be other than horizontal will then be considered.

3. Focusing Action of Horizontal Elongated Irregularities Above a Flat Earth

By assuming that the horizontal elongated irregularities are moving over a flat earth, we simplify the problem to the extent that all directions retain their identity when attention is transferred from the level of the irregularity to that of the observer. The three basic directions in the problem are the direction of the baseline reckoned from its southerly end to its northerly end, the direction of the radio source and the direction of movement of the focusing irregularity. At this stage it is assumed that the velocity of the irregularity is horizontal and normal to its larger dimension. These three directions are characterized by azimuths (measured from the north through east) σ (baseline), ξ_s (source) and v (velocity). For Casseopeia A as seen from Boulder, ξ_s lies between 317° and 43°, σ is constant (41°), and ν may have any value between 0° and 360°.

3.1. Geometry of the Refracted Ray

In figure 1 let SO be a ray propagating in a medium of refractive index $\mu+\delta\mu$ which encounters at 0 a boundary separating this medium from one of the refractive index μ. It will be refracted at 0 to propagate in the second medium along OP. Let OS′ be the continuation of PO, then the angle through which the ray is refracted is β_e. θ_s and ξ_s represent the zenith angle and azimuth of the incident ray while θ_e and ξ_e represent the zenith angle and azimuth of the refracted ray. A consideration of the spherical triangle ZSS′ yields the relationship

$$\cos(\xi_e-\xi_s)=(\cos\beta_e-\cos\theta_s\cos\theta_e)/\sin\theta_s\sin\theta_e. \quad (1)$$

An adaptation of Snell's law [Warwick, 1964] gives the approximate formula

$$\sin\beta_e=(\delta\mu/\mu)\tan\rho \quad (2)$$

where ρ is the angle of incidence of the ray SO. If we neglect the earth's magnetic field, the refractive index is given by

$$\mu^2=1-f_0^2/f^2$$

where f_0 is the plasma frequency and f the frequency of the propagating wave. Thus (2) may be rewritten as

$$\sin\beta_e=-\{f_0\delta f_0/(f^2-f_0^2)\}\tan\rho. \quad (3)$$

Here $(f_0+\delta f_0)$ is the plasma frequency in the medium in which the incident ray propagates and f_0 the plasma frequency in the medium in which the refracted ray propagates. For the values of f_0, δf_0, and f commonly encountered viz, 5 Mc/s, 0.3 Mc/s, and 30 Mc/s, $f_0\delta f_0/(f^2-f_0^2)$ is of the order of 0.002. Thus for values of ρ up to 88.5°, β_e is less than 2.5° and cos β_e equals one with an error of less than one part in a thousand. This error increases to one part in a hundred for values of ρ between 88.5° and 89°. Consequently, except for angles of incidence greater than about 89°, cos β_e may be equated to one with little loss of accuracy. Therefore (1) may be written

$$\cos(\xi_e-\xi_s)=(1-\cos\theta_s\cos\theta_e)/\sin\theta_s\sin\theta_e.$$

For the case where the radius of curvature is horizontal it can be shown that

$$\cos\theta_e=\mu\cos\theta_s/(\mu+\delta\mu).$$

This case is an accurate representation of the situation for rays passing through the edge of an ionospheric lens. Since $\delta\mu/\mu$ is of the order of -0.002, $\mu/(\mu+\delta\mu)$ is of the order of 1.002 and θ_e is virtually equivalent to θ_s. Thus cos $(\xi_e-\xi_s)$ is very close to unity. A detailed examination of $(1-\cos\theta_s\cos\theta_e)/\sin\theta_s\sin\theta_e$ for the range of values of θ_s involved in the observations (50° to 81°) shows that cos $(\xi_e-\xi_s)$ is equivalent to unity with an accuracy of better than 0.1 percent. Thus little error occurs if changes in azimuth on reflection are neglected except when ρ is nearly 90°, that is when the irregularities are viewed along their length.

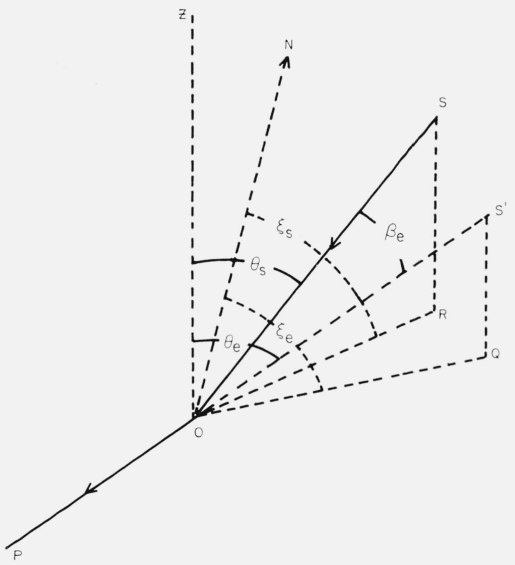

FIGURE 1. *Geometry of an incident and refracted ray SOP.*

3.2. Geometry of a Received Ray

In figure 2 let OSQ be a vertical plane containing the received ray SO which has an azimuth ξ and a zenith angle θ, OB is the direction of the interferometer baseline which has an azimuth σ. Then $\psi=\xi-\sigma$. Let YO be perpendicular to OB in the plane SOB. Then, φ is the complement of the angle measured by the interferometer, i.e., γ.

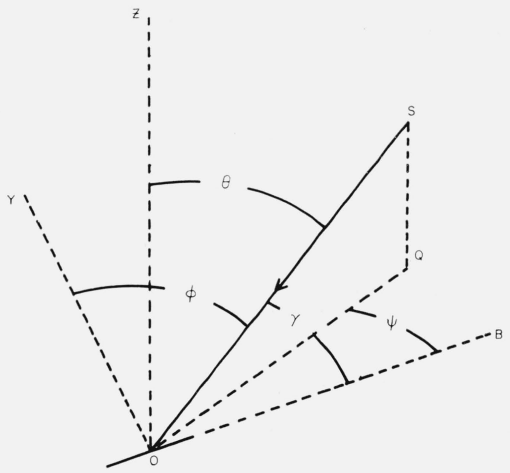

FIGURE 2. *Geometry of a received ray SO.*
OB is the baseline direction.

In the spherical triangle BSZ it can be shown that

$$\sin \varphi = \cos \gamma = \sin \theta \cos \psi.$$

When all such received rays have a constant azimuth it follows that small changes in θ, involved in moving from one ray to another, are related to the corresponding small changes in φ by

$$\delta\varphi = \delta\theta \cos \theta \cos \psi / \sin \gamma. \quad (4)$$

3.3. Edge Rays

In figure 3, DKL is the line image produced by the ionospheric lens whose long dimension is in the direction of CH and JI and whose short dimension is in the direction JC. The interferometer baseline is represented by MN (azimuth σ) and UFMK and WHNL are focused rays which pass through the interferometer antennas M and N. Since the direction of arrival varies monotonically across the baseline at a nearly uniform rate, the "average ray"

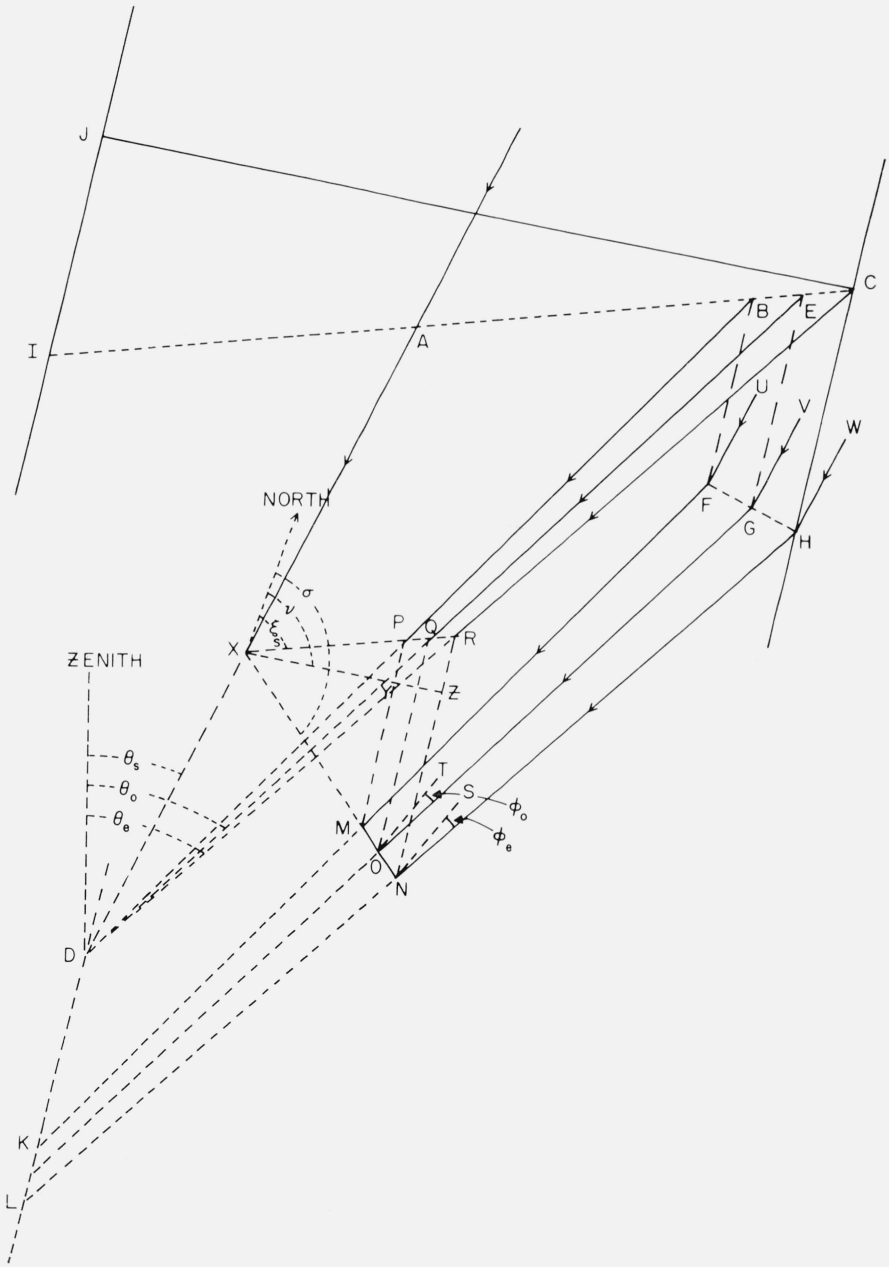

FIGURE 3. *Geometry of edge rays.*
The ionospheric lens JIHC produces the line image DKL.

to whose direction the interferometer responds is GO where O and G are the midpoints of FH and MN, respectively.

In section 3.1 it was shown that, except along the long dimension of an irregularity, the azimuths of rays from near the edge of the lens are unchanged from that of the source. Consequently FM, GO, and HN have the same azimuth as a ray which passes undeviated through the central portion of the lens (AX). However, the rays FM, GO, and HN do not necessarily meet at a point on the line image DL, since the azimuthal direction of the source and the baseline direction are, in general, skew.

Rays BP, EQ, and CR are parallel to FM, GO, and HN respectively, in the vertical cut of the lens IACD which has the same azimuth as the source (ξ_s). Rays BP, EQ, and CR are obtained from FM, GO, and HN by projecting along the direction of the long dimension of the lens. Then BP, EQ, and CR necessarily intersect on the line image in a point D and θ_s, θ_0, and θ_e are thus the zenith angles of the source (i.e., the undeviated ray AD, EQ (or GO) and CR (or HN) respectively. Line PQR is the projection of the baseline on the azimuthal plane IACD, while XYZ is parallel to the short dimension of the irregularity JC (azimuth ν) and is therefore normal to RN.

Let SN be perpendicular to MN in the plane MNH and TO perpendicular to MO in the plane MOG. Thus φ_e and φ_0 are the complements of the angles which the interferometer would measure for the directions HN and GO. Let φ_s be the complement of the angle the interferometer would measure if the source were viewed directly in the absence of the lens.

Considering the projection of MN on XR we have

$$\mathrm{PR}=\mathrm{MN}\cos(\sigma-\nu)/\cos(\nu-\xi_s)=\Delta\cos(\psi-\kappa)/\cos\kappa$$

where $\psi=\sigma-\xi_s$, $\kappa=\nu-\xi_s$ and Δ is the length of baseline. Detailed examination of this relationship for all values of ξ_s and ν shows that it is independent of the magnitude of ν but changes sign when ξ_s is larger than 180°. Therefore, in general

$$\mathrm{PR}=\pm\Delta\cos(\psi-\kappa)/\cos\kappa \qquad (5)$$

where the positive sign applies for $\xi_s<180°$ and the negative sign applies when $\xi_s>180°$.

Considering the edge ray HN and the average ray GO, it can be seen that

$$(\varphi_e-\varphi_s)-(\varphi_0-\varphi_s)=\varphi_e-\varphi_0.$$

Since φ_e is very little different from φ_s or φ_0, use can be made of (4) to produce the following:

$$(\theta_e-\theta_s)\cos\theta_s\cos\psi/\sin\gamma_s-(\varphi_0-\varphi_s)$$

$$=(\theta_e-\theta_0)\cos\theta_s\cos\psi/\sin\gamma_s, \qquad (6)$$

$\theta_e-\theta_s$, $\varphi_0-\varphi_s$ and $\theta_e-\theta_0$ are functions of frequency $\theta_e-\theta_s$ will be written $\delta\theta_e(f)$ and $\varphi_0-\varphi_s$ as $\delta\varphi_0(f)$ or $-\delta\gamma_0(f)$. $\delta\gamma_0(f)$ is the change in the apparent position of the source, as measured by the interferometer, as the edge of the irregularity just comes into view; $\theta_e-\theta_0$ can be determined as a function of frequency as follows.

In figures 4a and 4b we have drawn the vertical plane through the source for observing frequencies (f) larger than the focus frequency (f_m) and smaller than the focus frequency. The focus frequency is defined [Warwick, 1964] as the frequency for which the focal length of the ionospheric lens [$F(f)$] equals its range (d). It can be seen from figures 4a and 4b that

$$\theta_e-\theta_0=\pm\mathrm{PR}/2\{F(f)-d\}$$

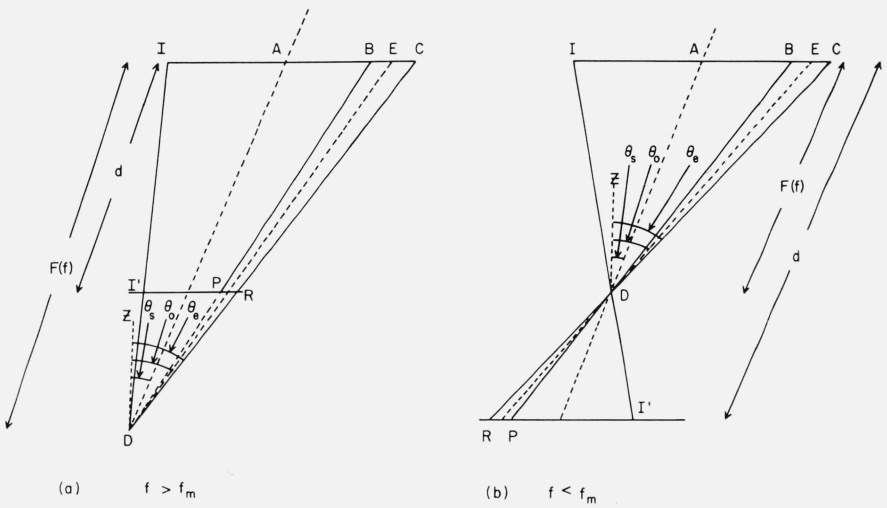

FIGURE 4. *Illustrating the relationship between* θ_e *and* θ_o *and the focal length* F(f) *and range d of an irregularity for* (*a*) $f>f_m$ *and* (*b*) $f<f_m$.

where the positive sign applies to the case $f>f_m$ and the negative sign to the case $f<f_m$. In what follows only the case $f>f_m$ will be considered. With (5), (6) can now be written

$$\delta\theta_e(f)\cos\theta_s\cos\psi/\sin\gamma_s+\delta\gamma_0(f)$$

$$=\pm\frac{\Delta}{2\{F(f)-d\}}\cdot\frac{\cos(\psi-\kappa)}{\cos\kappa}\cdot\frac{\cos\theta_s\cos\psi}{\sin\gamma_s}. \quad (7)$$

Since the refraction of edge rays results in changes in zenith angle rather than azimuth (sec. 3.1), and even these changes are small, (3) may be written

$$\delta\theta_e(f)=-\{f_0\delta f_0/(f^2-f_0^2)\}\tan\rho$$

or

$$\delta\theta_e(f)\propto 1/(f^2-f_0^2).$$

It follows that

$$F(f)\propto(f^2-f_0^2) \quad (8)$$

where $F(f)$ is the focal length of the lens. However, for most cases, f is an order of magnitude larger than f_0 and thus

$$F(f)=df^2/f_m^2 \quad (9)$$

where d is the focal length and the range of the irregularity at the focus frequency f_m.

The angle measured by the interferometer γ is given by

$$\cos\gamma=(nc/f+p)/\Delta$$

where n is the fringe order, c the velocity of light, f the observing frequency, p the difference in length of the two antenna feeders and Δ the length of the baseline. It follows that

$$\delta\gamma=nc\delta f/f^2\Delta\sin\gamma \quad (10)$$

where $\delta\gamma$ is the shift in the measured angle corresponding to an observed shift of δf in the frequency at which a given fringe order is excited. Since $n=f/\Delta f$ where Δf is the fringe spacing, (10) can be written

$$\delta\gamma=(c/f\Delta\sin\gamma)(\delta f/\Delta f). \quad (11)$$

Using (9) and (11), it is possible to rewrite (7) as follows

$$f\frac{\delta f}{\Delta f}=a\frac{f^2f_m^2}{(f^2-f_m^2)}\div b$$

where

$$a=\pm\frac{\Delta^2}{2cd}\frac{\cos(\psi-\kappa)\cos\theta_s\cos\psi}{\cos\kappa} \quad (12)$$

and

$$b=-(\Delta/c)f^2\delta\theta_e(f)\cos\theta_s\cos\psi. \quad (13)$$

The positive sign in the expression for a applies if $\xi_s<180°$ and the negative if $\xi_s>180°$. Since $\delta\theta_e(f)$ is proportional to f^2 it follows that $f^2\delta\theta_e(f)$ is constant and so all the quantities involved in the expressions for a and b are constants for a particular scintillation.

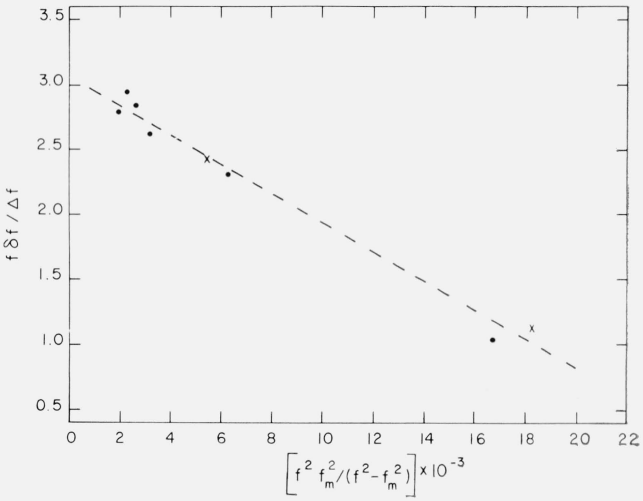

FIGURE 5. *Scatter diagram showing the connection between* $f\delta f/\Delta f$ *and* $f^2 f_m^2/(f^2-f_m^2)$ *for the scintillation at 0710 UT, 14 December, 1960.*

Thus $f\delta f/\Delta f$ should be a linear function of $f^2f_m^2/(f^2-f_m^2)$. This has been verified for a number of scintillations. Figure 5 shows the plot of $f\delta f/\Delta f$ versus $f^2f_m^2/(f^2-f_m^2)$ for the scintillation at 0710 hr UT on 14 December 1960 which was discussed in detail by Warwick [1964]. The value of f_m used (28 Mc/s) was obtained by an interpolation between the fringe slopes on either side of the fringe-slope changeover, relative to the star's diurnal motion. It will be noted that the expression for a, (12) contains the range of the irregularity d. Unfortunately evaluation of a does not lead immediately to d since the direction of movement of the irregularity and hence κ are unknown.

The following consideration of figure 6 will yield expressions for the duration of the scintillation and the width and velocity of the focusing irregularity. The duration $t(f)$ of a scintillation at frequency f is given by

$$t(f)=D\cos\kappa/v$$

where v is the irregularity, and hence the image, velocity, D is given by

$$D=\pm\ell\{F(f)-d\}/F(f)=\pm\ell(f^2-f_m^2)/f_m^2$$

where the positive sign applies to the case $f>f_m$ (fig. 6) and the negative sign to the case $f<f_m$. Thus

$$t(f)=\pm\ell\cos\kappa(f^2-f_m^2)/vf^2.$$

As f increases (in the $f>f_m$ case), $t(f)$ reaches a limiting value t_i and in terms of this

$$t(f)=\pm t_i(f^2-f_m^2)/f^2. \quad (14)$$

Thus as frequency increases $t(f)$ decreases from extremely large values for small values of f to zero at f_m and increases again to t_i for large values of f.

734-668—64——3

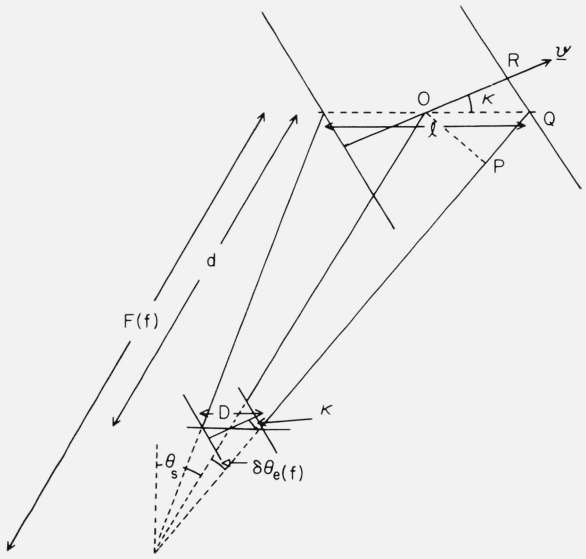

FIGURE 6. *This figure illustrates the derivation of expressions for speed of movement (ν) and irregularity width (ℓ).*

This offers an explanation for the narrowing of the scintillation near f_m as reported in part I.

From figure 6 it is evident that the breadth of the focusing irregularity (L) is given by

$$L=2 \text{ OR}=2 \text{ OP} \cos \kappa/\cos \theta_s=2F(f)\delta\theta_e(f) \cos \kappa/\cos \theta_s$$

i.e.,

$$L=2d\delta\theta_e(f_m) \cos \kappa/\cos \theta_s. \tag{15}$$

Making use of (13) this becomes

$$L=-2bcd \cos \kappa/f_m^2\Delta \cos^2 \theta_s \cos \psi. \tag{16}$$

All the quantities but κ on the righthand side of this equation are obtainable for any scintillation and thus L cannot be calculated without a knowledge of the direction of movement of the irregularity.

The magnitude of the irregularity velocity is obtained directly from a knowledge of L and t_i since

$$\nu=L/t_i=-2bcd \cos \kappa/t_i f_m^2\Delta \cos^2 \theta_s \cos \psi. \tag{17}$$

Again a lack of knowledge of κ prevents evaluation of ν.

3.4. Apparent Angular Drift of the Source

As a focusing irregularity moves across the line of sight of the radio star it will change the apparent position of the star in a definite pattern, as explained by Warwick [1964]. In this section an expression will be derived for the rate of change of the observed angular position of the source. At the beginning of a scintillation the observed angular position of the source changes abruptly from γ_s to $\gamma_0(f)$ (for the edge ray) that is by an amount $\delta\gamma_0(f)$. There is then a gradual recovery to γ_s and then a gradual overshoot to $\gamma_s-\delta\gamma_0(f)$. Thus the total change in the apparent angular position of the source is $2\delta\gamma_0(f)$ and this occurs in a time $t(f)$. The rate of change of the observed angular position of the source $W_0(f)$ is consequently given by

$$W_0(f)=2\delta\gamma_0(f)/t(f).$$

From (7), (9), (14), and (15), $W_0(f)$ can be written finally as

$$W_0(f)=\frac{\nu f_m^2}{(f^2-f_m^2)}\left\{\frac{\cos \theta_s \cos (\xi_s-\sigma)}{d \cos \gamma_s}\right\} \left\{\frac{-\cos \theta_s \pm \frac{\Delta}{L}\frac{f^2}{f^2-f_m^2} \cos (\nu-\sigma)}{\cos (\xi_s-\nu)}\right\} \tag{18}$$

where the positive sign before the second term applies if ξ_s is less than 180° and the negative if ξ_s is larger than 180°. This expression applies for $f>f_m$ but can be converted into the analogous expression for the case $f<f_m$ by reversing the signs before the second term.

At frequencies higher than the focus frequency, the CB_H and CA_H type scintillations involve values of $W_0(f)$ which are of opposite sign. It is instructive, therefore, to examine the variations of $W_0(f)$ with source azimuth ξ_s and wind azimuth ν. In figure 7 the full line and dashed curves represent $W_0(f)$ $(f^2-f_m^2)/f_m^2$ plotted against source azimuth for several values of the wind azimuth. Here f has been taken as $1.2f_m$, L given the value 5 km, and only the range of azimuths and elevations appropriate to the observations of part I have been considered. The curves have an infinity when $\xi_s=\nu-90°$. Under this condition the irregularity is being viewed along its long dimension and its focusing action will be such as to produce changes in azimuth rather than elevation. However, the approximation on which the curves of figure 7 are based assumes that the focusing action involves changes in elevation only (sec. 3.1). Thus the infinities in the curves at $\xi_s=\nu-90°$ are unlikely to be meaningful.

To interpret correctly the curves of figure 7 it is essential to know over which parts of the curves the approximation on which they are based is accurate. An accuracy criterion for these curves can be established in the case where the normal to the refracting surface, where an edge ray strikes it, is horizontal. In this case it can be shown readily that

$$\cos \rho=\sin \theta_s \cos (\nu-\xi_s). \tag{19}$$

It was pointed out in section 3.1 that it is reasonable to assume that there is negligible change in azimuth on refraction when $\cos \beta_e$ is approximately equal to one, that is when ρ is less than 88.5°. Using this limitation on ρ it is possible to employ (19) to find the range of values of ξ_s, for each ν, for which the approximation used in the construction of figure 7 is

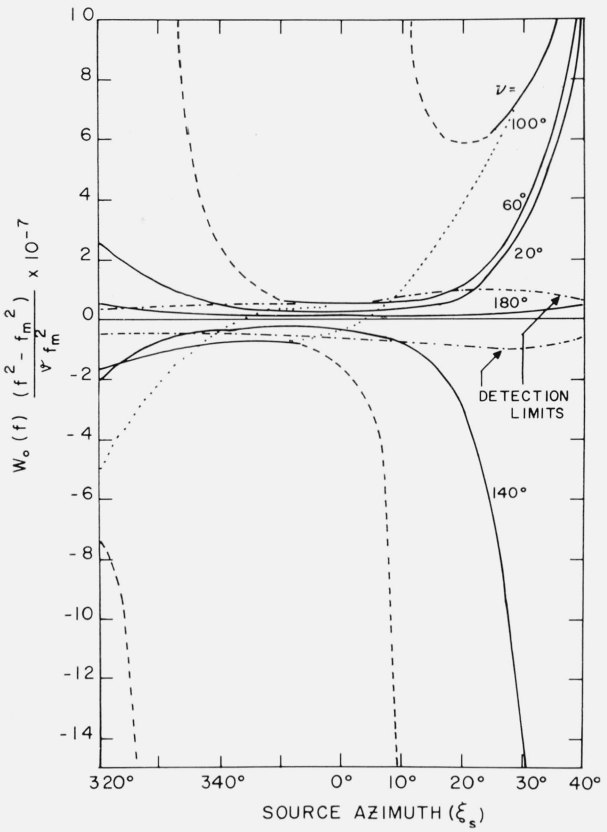

FIGURE 7. *Variation of the rate of change of the observed angular position of a refracted ray with source azimuth* (ξ_s) *for several values of wind azimuth* (ν).

accurate (full lines). As anticipated, the approximation, based on no change in azimuth on refraction, breaks down (dashed lines) in the vicinity of the infinities at which the sign of $W_0(f)(f^2-f_m^2)/f_m^2$ changes. Thus, in those cases where $W_0(f)(f^2-f_m^2)/\nu f_m^2$ changes sign it is only possible to determine part of the curve which represents the variation of this quantity with ξ_s. A complete theory would, of course, allow all the curve to be determined. Lacking such a theory, we assumed that a connection between the two branches of the curve, consistent with the curvature trends of the branches, approximates to the true variation. These connections are drawn as dotted lines on figure 7.

It can be shown that

$$W_0(f)\,\frac{(f^2-f_m^2)}{\nu f_m^2}=\frac{2c}{L\Delta\sin\gamma_s}\cdot\frac{f}{f_m^2}\cdot\frac{\delta f}{\Delta f}. \qquad (20)$$

Assuming that the smallest detectable value of δf is ± 0.1 Mc/s, we can determine how the smallest detectable value of $W_0(f)(f^2-f_m^2)/\nu f_m^2$ varies with ξ_s. The dash-dotted lines of figure 7 represent this variation for an f_m of 30 Mc/s and an f of 36 Mc/s.

In a CB_H [Singleton, 1964] scintillation the fringe drift is from high to low frequency as time progresses. Now

$$\cos\gamma_0(f)=nc/f\Delta+p/\Delta.$$

If n is kept constant and nonzero and f allowed to decrease, obviously $\gamma_0(f)$ decreases. But $W_0(f)$ is equivalent to $d\gamma_0(f)/dt$ so that CB_H scintillations are associated with negative values of $W_0(f)$. A similar argument shows that CA_H scintillations are associated with positive values of $W_0(f)$. From diagrams such as figure 7 it is possible, therefore, to determine the ranges of values of source azimuth (ξ_s) over which detectable CB_H and CA_H scintillations will be produced by a given wind azimuth (ν). Scintillations occurring at those values of ξ_s and ν for which $W_0(f)$ is below the limit of detection will correspond to type N as defined in part I. A summary of the ranges of values of ξ_s over which CB_H, CA_H, and N type scintillations would be expected for a full range of values of ν is presented in the lower part of figure 8. The upper two histograms in figure 8 show how the occurrence of CB_H and CA_H scintillations vary with source azimuth. They show that there is a changeover from CB_H to CA_H at a source azimuth of about 8°. Such a change is predicted most accurately by a wind azimuth of 120°.

In order to gain more information about the direction of the wind, an attempt has been made to re-

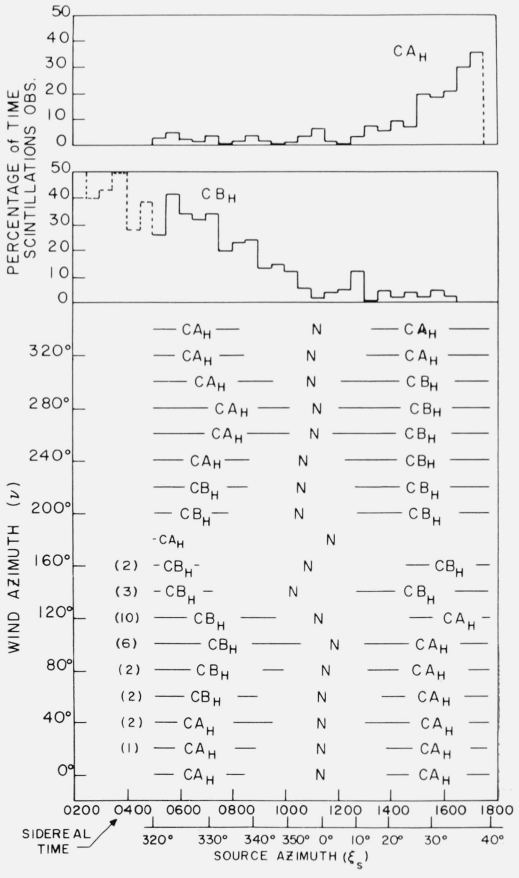

FIGURE 8. *The theoretical predictions of position shift properties of scintillations (lower figure) are here compared with the experimentally determined histograms of CB_H and CA_H occurrence (upper histograms).*

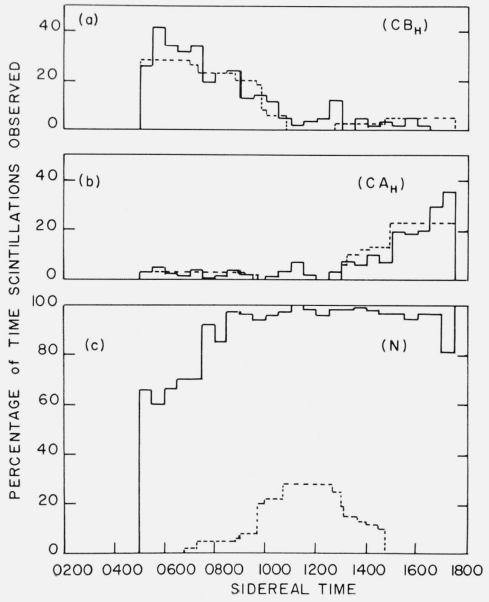

FIGURE 9. *Predicted histograms (broken lines) of (a) CB_H, (b) CA_H and (c) N type scintillations compared with the experimental histograms (full lines).*

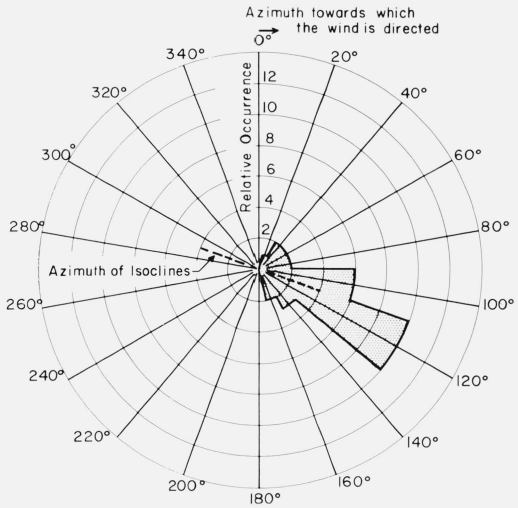

FIGURE 10. *A polar plot of the relative occurrence of wind azimuths.*

construct the experimental histograms of CB_H and CA_H occurrence versus sidereal time. This was done by allotting weights to the predictions of figure 8 for wind azimuths of 20° to 160°. The weights (numbers in brackets on fig. 8) were chosen by trial and error so as to get reasonable agreement between prediction and experiment for the CB_H and CA_H histograms. Figures 9a and 9b compare the experimental (full line) and predicted (broken line) histograms for CB_H and CA_H scintillations.

Using the weights employed in the construction of figure 8, we can gain some idea of the variation of the relative occurrence with wind azimuth (fig. 10). Figure 10 also shows the azimuth of the isoclines in the observing region. It would appear that irregularities producing CB_H and CA_H type scintillations are usually elongated in the magnetic north-south direction, the component of motion normal to their length lying towards the southeast along the isoclines.

Reverting to figures 8 and 9, we expect that the adopted weighting procedure would also reproduce the observed sidereal time variation of occurrence of the N condition. Figure 9c shows that this is not the case. However, it is interesting to note that the synthetic histogram (broken line), though smaller and narrower than the observed (full line) histogram reproduces, to some degree, the trends of the observed histogram. Note especially the slower rise of occurrence than fall off of occurrence with increasing sidereal time. From (20) it will be seen that a decrease of f_m by a factor of three increases the minimum detectable value of $W_0(f)\ (f^2-f^2_m)/f^2_m$ by an order of magnitude. Such a change increases the range of ξ_s over which N type scintillations may be observed at the expense of CB_H and CA_H scintillations. Thus the synthetic histogram of figure 9c may be widened and increased in height to fit the observed histogram more closely if it is assumed that values of f_m lower than 30 Mc/s predominate. The relative heights of the synthetic and observed histograms suggest that the number of occasions when $f_m<30$ Mc/s to the number when $f_m>30$ Mc/s should be of the order of 2 to 1.

4. Effect of a Spherical Earth and Ionosphere and Nonhorizontal Irregularities

The above discussions have been based on the approximation that the earth and ionosphere are flat. Little change in the form of the analysis is necessary when a change is made to a spherical earth and ionospheric situation. The main difficulty that arises is that the azimuth of a vector at a point other than on the observer's zenith cannot be transferred without change to the observing point. This is due to the convergence of meridians. Computations have been made which allow the assessment of the error involved in assuming that the apparent azimuth (as seen from the ground) of a vector in the ionosphere equals its true azimuth in the ionosphere. These computations are summarized in figure 11 where the error for several true azimuths is plotted against sidereal time. An irregularity height of 300 km has been assumed. It will be seen that the error never exceeds 3.2°. Considering the crude method used to determine the wind direction in section 3.4, an error of this magnitude is probably of little significance.

So far the irregularities have been assumed to be elongated and horizontal and are thus similar to those thought to be responsible for some types of midlatitude spread-*F* [Bowman, 1959]. There is a considerable bod of evidence however, which points to the

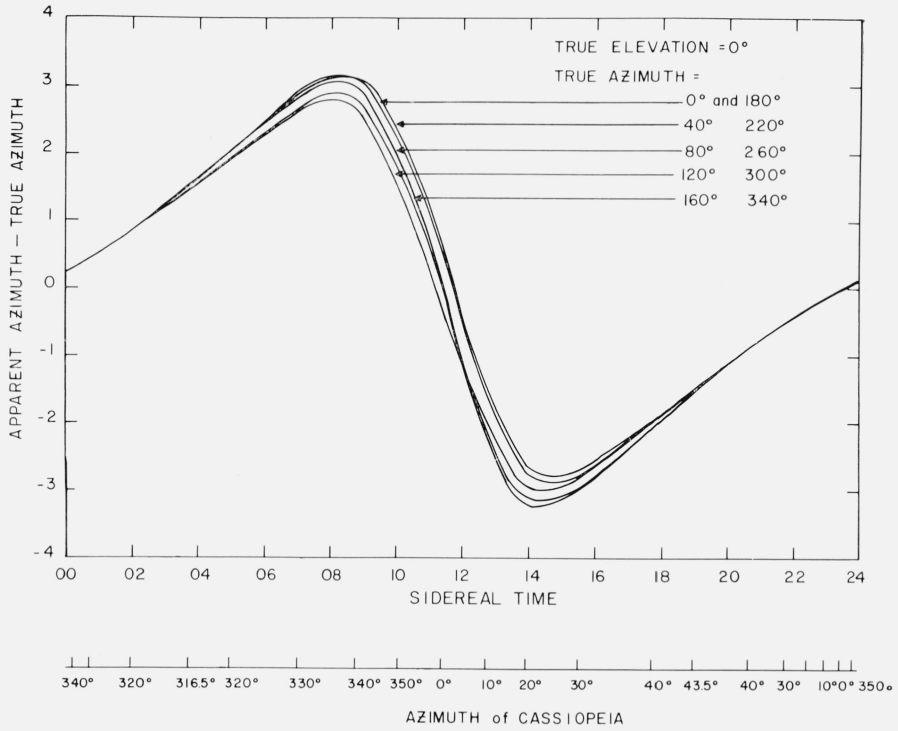

FIGURE 11. *Error involved in assuming that the apparent azimuth of a vector at a distant point in the ionosphere is equal to its true azimuth at that point, plotted against sidereal time.*

existence of large field-alined irregularities at these latitudes [Peterson et al., 1955; Dearden, 1962; Knecht and Russell, 1962]. Such irregularities, if they exist in the form of columns, would appear to be suitable focusing structures. Since a region where the dip is of the order of 75° is being viewed at zenith angles ranging from about 60° to 80°, the geometrical problem reduces to one similar to that already considered except that the equivalent irregularities are effectively near the zenith. It does not seem possible to distinguish between these models with the experimental information available and the present state of the theory.

5. Intensity of Focused Scintillations

In the vicinity of the focus the beam of radiation focused by an ionospheric irregularity will have a cross section smaller than that of the irregularity. As a result the signal strength in the focused beam, near the focus, will be higher than the signal strength at the same point in the absence of the focusing irregularity. The gain in signal strength as the result of focusing can be calculated as follows.

Consider figures 4a and 4b. The radiation which passes through an area of breadth AB reaches the ground over an area of the same length as the irregularity but with a breadth CD. The gain (G) in signal strength is obviously:

$$G=\frac{AB}{CD}=\pm\frac{F(f)}{F(f)-d} \qquad (21)$$

where the positive sign applies to the case where $f>f_m$ and the negative to the case where $f<f_m$. Use (8) to evaluate $F(f)$; then (21) becomes

$$G=(1-f_0^2/f^2)/|1-f_m^2/f^2|.$$

In figure 12 the gain is plotted as a function of f_m/f for several values of f_0/f. The broken line parts of the curves represent the situation where f_m is not greater than the critical frequency of the F-layer (f_0). This is physically unlikely. Note the limited

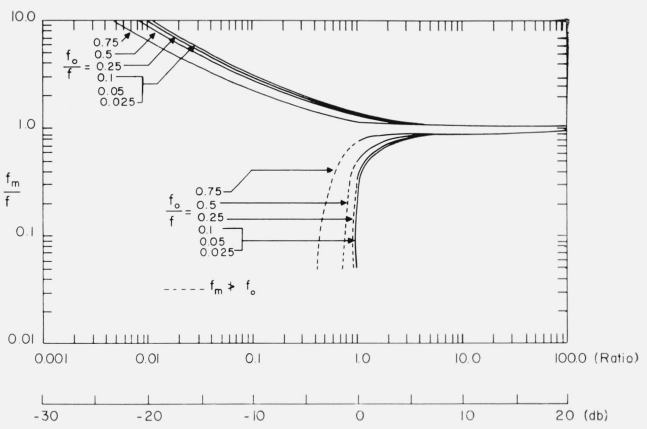

FIGURE 12. *Gain due to the focusing action of an ionospheric lens plotted against* f_m/f *for several values of* f_0/f.

range, about f_m, of observing frequency (f) for which the gain is greater than one. Bandwidths up to 7:1 are possible when the F-layer critical frequency f_0 is less than 10 percent of the observing frequency f. This upper limit to the bandwidth drops to 1.6 to 1 for f_0 equal to 75 percent of f. The observed bandwidths (part I) of 2:1 and occasionally 3:1 are consistent with this result.

In figure 13, f_m/f is plotted against f_0/f for a gain of one. Gains greater than one occur only for values of f_m/f and f_0/f which correspond to points within this curve. On the left and bottom of the figure several scales of observing frequency f have been added for particular values of f_m and f_0. The effective band of the swept-frequency interferometer (after the MUFE has been taken into account) is shown on these scales by the thick lines. It is evident that some or all of a scintillation whose focus frequency f_m fulfills the condition 2 Mc/s$>f_m>$56 Mc/s may be observed with the interferometer.

Figure 13 offers an explanation for those scintillations which exist only in the low-frequency octaves. Consider a focus frequency of 5 Mc/s and an F-layer critical frequency of 2 Mc/s. As the observing frequency (f) is allowed to vary from 10 to 40 Mc/s, curve (a) is traced out. It can be seen that under these conditions the gain is greater than one only for f less than 25 Mc/s. For the same value of f_m but a higher value of f_0, say 4 Mc/s, curve (b) shows that, only for observing frequencies less than 20 Mc/s, the gain will be greater than one. Thus low-frequency scintillations apparently occur when f_m and f_0 are small. Low values of f_0 will be associated with the low values of MUFE necessary to permit observation of low-frequency scintillations. However, as found experimentally in part I, low values of MUFE, while a necessary condition for the observation of low-frequency scintillations, is not a sufficient condition. The focusing frequency must also be small.

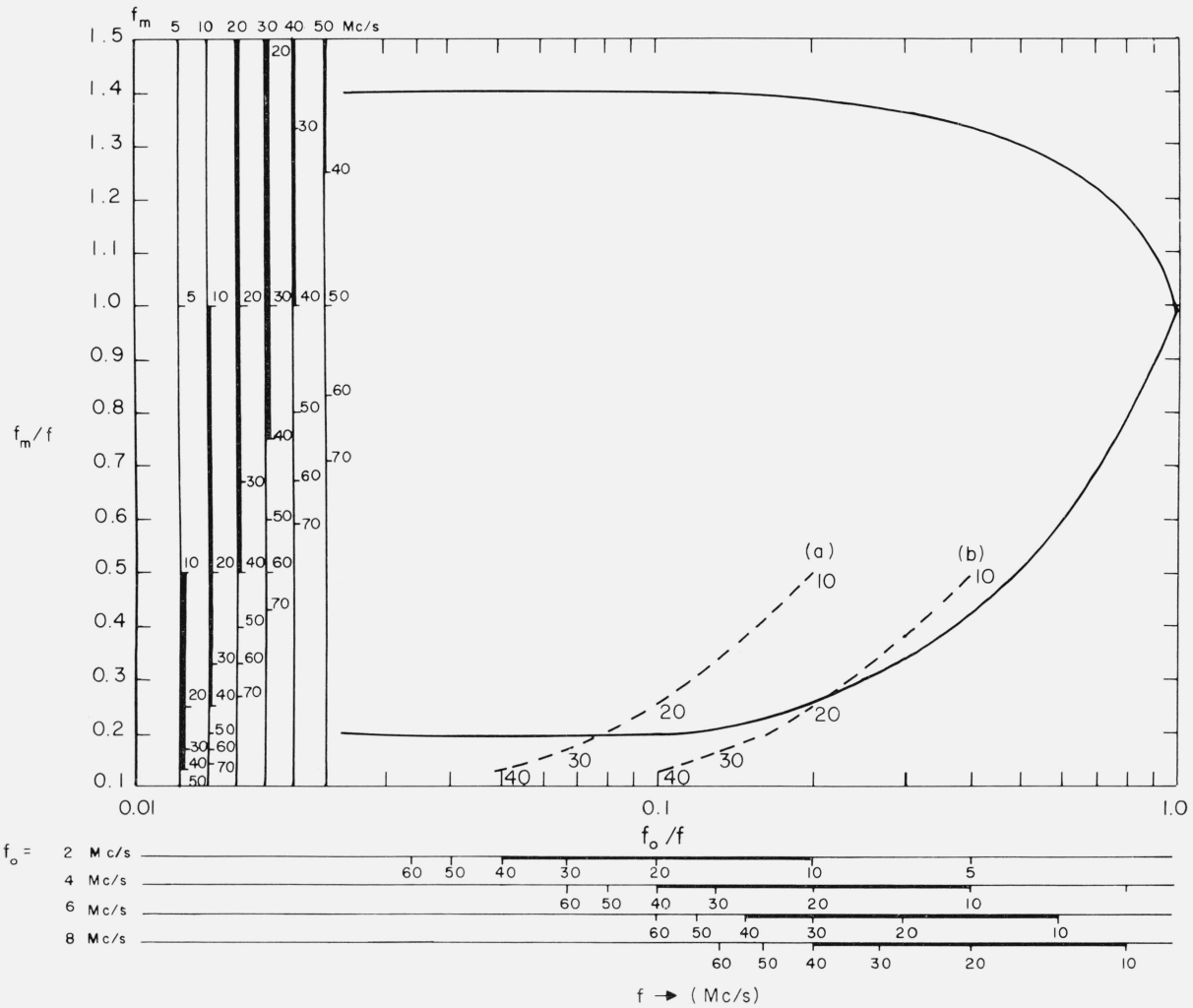

FIGURE 13. *Here* f_m/f *is plotted against* f_0/f *for a focusing-action gain of one (full-line curve).*

Several f scales for particular values of f_m and f_0 are also included. The broken-line curves show the variation of f_m/f with f_0/f for (a) f_m= 5 Mc/s and f_0=2 Mc/s, and (b) f_m=5 Mc/s and f_0=4 Mc/s as f varies from 10 to 40 Mc/s.

6. Association Between Focusing Frequency and Spread-*F* Parameters

The focusing properties of an ionospheric irregularity depend on its incremental electron density, its size and the nature of the curvature of its surfaces. By assuming that the irregularities which produce scintillations are the same as those which simultaneously produce spread-*F*, it is possible to gain information about the incremental electron density of the scintillation-producing irregularities.

Conventional ray optics will now be used to develop connections between the focusing frequency of an irregularity and its incremental electron density. Three curvature models will be considered. In the first model the irregularities will be assumed to be semicylindrical deviations from isoionic contours that are otherwise flat. Cylindrical columns will be considered as the second model. In the third model the isoionic contours will be assumed to have a sinusoidal wavelike nature.

6.1. Semicylindrical Irregularities

Figure 14a depicts an irregularity which takes the form of a semicylindrical deviation of an otherwise flat isoionic contour. It will be assumed that the refractive index immediately beneath the contour is μ, while that immediately above is $\mu+\delta\mu$. The irregularity, which has a radius of curvature r, is at a distance d from the observing point. It is well known [Longhurst, 1957] that the focal length (F) of such a system is given by

$$\frac{\mu}{F}=\frac{\mu-(\mu+\delta\mu)}{r} \tag{22}$$

Neglecting the effect of the earth's magnetic field, the refractive index of a plasma for an observing frequency f is given by

$$\mu^2=1-f_0^2/f^2 \tag{23a}$$

and

$$(\mu+\delta\mu)^2=1-(f_0+\delta f_0)^2/f^2 \tag{23b}$$

where f_0 is the plasma frequency below the boundary in figure 4a and $f_0+\delta f_0$ is the plasma frequency above this boundary. Using these two expressions in connection with (22) and assuming that the radius of curvature is at least an order of magnitude smaller than the focal length, we find that

$$(r/F)(f^2-f_0^2)=2\delta f_0 f_0+\delta f_0^2. \tag{24}$$

The variation of plasma frequency at the peak of the F-layer associated with most spread-F configurations is an order of magnitude less than the minimum plasma frequency here. Thus (24) can be written

$$\delta f_0/f_0=(r/2F)\{(f/f_0)^2-1\}.$$

When the observing frequency f equals the focus frequency f_m the focal length F equals the range d of the focusing irregularity. Thus

$$\delta f_0/f_0=(r/2d)\{(f_m/f_0)^2-1\} \tag{25}$$

which is the required connection between the focusing frequency and the parameters of the associated spread-F configuration.

If, as in figure 14a, the irregularity is convex as viewed from below, d and r are required to have

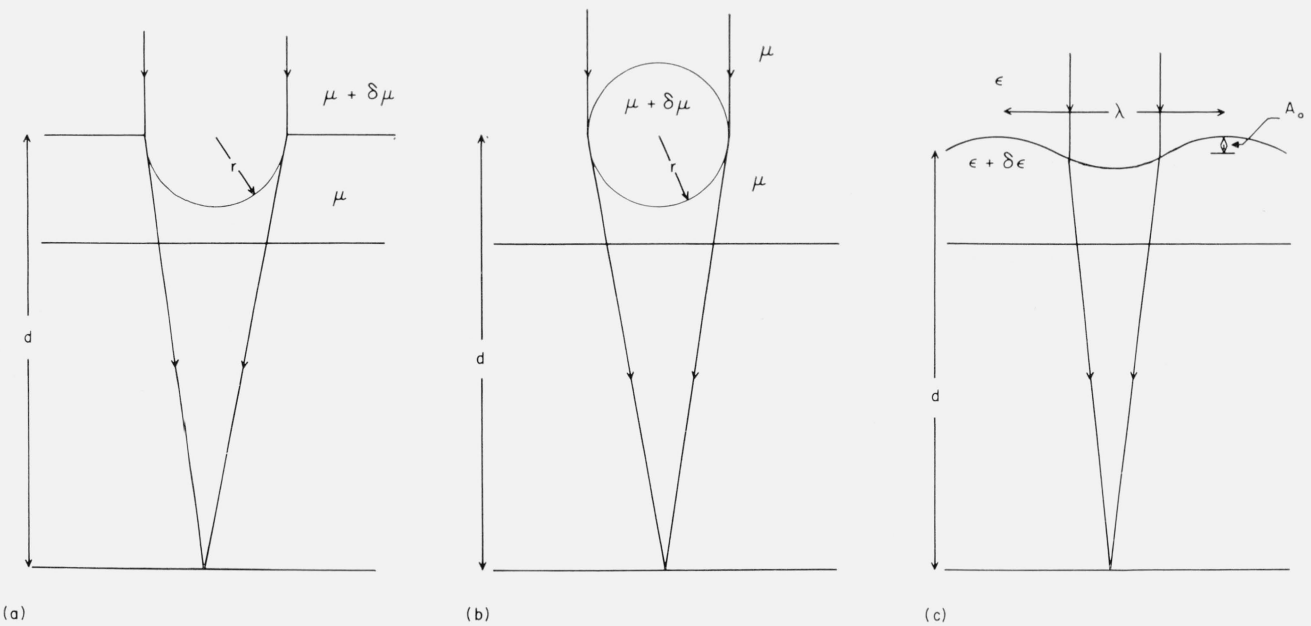

FIGURE 14. *The three irregularity models whose focusing properties have been investigated.*

opposite sign (according to the sign convention used) to enable the lens to be convergent and thus δf_0 is negative. If the irregularity is concave as viewed from below δf_0 has to be positive for the lens to be convergent.

6.2. Cylindrical Irregularities

The focusing action of a cylindrical irregularity in a plane normal to its axis will now be considered. Assuming that the irregularity has a circular cross section of radius r and that the refractive index of the plasma within the irregularity is $\mu+\delta\mu$ and that outside μ (fig. 14b), simple ray optics [Longhurst, 1957] can be used to show that the focal length F is given by

$$\frac{2F}{r}-1=\frac{\mu}{\delta\mu}$$

where F and r have to be of opposite sign for the lens to be convergent. Since F is expected to be at least an order of magnitude larger than r, this may be rewritten

$$2F/r=\mu/\delta\mu, \tag{26}$$

which is of similar form to (22). Employing the methods outlined in section 6.1, but using (26) rather than (22), we obtain the following connection between the focusing frequency, range of the irregularity and the parameters of the associated spread-F.

$$\frac{\delta f_0}{f_0}=-\frac{r}{4d}\{(f_m/f_0)^2-1\}. \tag{27}$$

Here d and r have to be of opposite sign for the lens to be convergent, and hence δf_0 is negative.

6.3. Sinusoidal Irregularity

Warwick [1964] considered the focusing action of irregularities resulting from sinusoidal wavelike isoelectronic contours. Such irregularities are depicted in figure 14c. He demonstrated that rays passing through the lens at points distant $|y|$ from its axis are brought to a focus at a distance f given by

$$f=(\lambda/2\pi L)y/(\sin 2\pi y/\lambda)$$

where $L=\delta\epsilon A_0/2\epsilon$ and A_0, λ, and the dielectric constants ϵ and $\epsilon+\delta\epsilon$ are as shown in figure 14c. Because of the caustic effect associated with such lenses, Warwick asserts that the rays passing through the edge of the circle of least confusion arise from the points $y=\pm\lambda/10$, and the effective focal length is thus

$$F=\frac{\lambda^2}{5.878\pi A_0}\cdot\frac{\epsilon}{\delta\epsilon}.$$

Since $\epsilon=n^2=1-f_0^2/f^2$, it follows that

$$\delta\epsilon/\epsilon=-(2\delta f_0/f_0)/\{(f/f_0)^2-1\}$$

and thus

$$F=\frac{\lambda^2}{5.878\pi A_0}\cdot\frac{(f^2/f_0^2)-1}{2\delta f_0/f_0}.$$

At the focus frequency (f_m), F equals the range of the irregularity (d). Consequently, the final connection between the focus frequency, the range and dimensions of the irregularity, and the parameters of the associated spread-F configuration is

$$\frac{\delta f_0}{f_0}=\frac{\lambda^2}{36.9A_0}\cdot\frac{1}{d}\left\{\left(\frac{f_m}{f_0}\right)^2-1\right\}. \tag{28}$$

6.4. Experimental Verification

In sections 6.1, 6.2, and 6.3 it has been demonstrated that the relationship between the focus frequency (f_m), the range of the irregularity (d) and the parameters of the associated spread-F configuration (f_0 and δf_0) is

$$\frac{\delta f_0}{f_0}=\frac{s}{d}\left\{\left(\frac{f_m}{f_0}\right)^2-1\right\} \tag{29}$$

where s is a function of the size and shape of the irregularity. In part I, figure 15, it was shown that $f_0\delta f_0$ is proportional to f_m^2. This is consistent with (29) since f_m is usually an order of magnitude larger than f_0. The same body of data in part I, figure 15, is used in a scatter plot (fig. 15) of $\delta f_0/f_0$ versus $\{(f_m/f_0)^2-1\}$. A linear relationship obviously exists, the correlation coefficient of the scatter being 0.79 with a 1 percent confidence level of 0.41. The slope of the line fitted to the scatter is 8.57×10^{-4}.

Irregularities at 400 km viewed between 1400 and 1700 hr sidereal time are at a range (d) of 930 km on the average. It follows that s equals 0.80 km on the average. Values of the breadth of the average focusing irregularity can be calculated in terms of s.

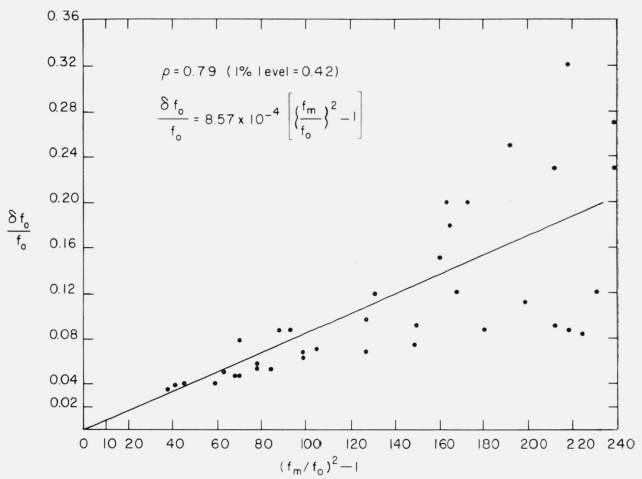

FIGURE 15. *The scatter diagram obtained when* $\delta f_0/f_0$ *is plotted against* $(f_m/f_0)^2-1$.

These calculations are summarized in table 1. In the case of the sinusoidal irregularity two widths are quoted. The first of these is calculated on the basis that the wavelength of the isoelectronic contour is comparable with its amplitude as assumed by Warwick [1964]. The second width quoted is based on the assumption that the depth of the focusing part of the irregularity is half its width, a situation which is directly comparable with the case of the semicylindrical irregularity.

The radius of the first Fresnel zone at a range of 930 km for the wavelengths used in most of the observations is 2.5 to 3.5 km. Thus it appears that the irregularities must be either of the cylindrical or sinusoidal types in order to be larger than this zone and allow refraction effects to dominate possible diffraction effects.

TABLE 1. *Comparison of the irregularity width for the three models proposed*

Semicylindrical irregularity	Cylindrical irregularity	Sinusoidal irregularity
$S=r/2=0.80$ km	$S=r/4=0.80$ km	$S=\lambda^2/36.9\ A_0=0.80$ km
$r=1.6$ km	$r=3.2$ km	$\lambda^2/A=29.5$
Width of irreg. $L=2r=3.2$ km	Width of irreg. $L=2r=6.4$ km	Width of irreg. $L=\lambda/2=14.7$ km ($A_0=\lambda$) $=\lambda/2=3.7$ km ($A_0=\lambda/4$)

7. Dispersion

As Wild and Roberts [1956] first suggested, the dispersion effects noted in part I are apparently due to horizontal gradients in electron density which act as huge prisms. Since scintillations with dispersion exhibit much the same position-shift properties as other broadband scintillations, focusing structures of the types discussed above as well as horizontal gradients are required for their explanation.

No complete analysis of dispersion by horizontal gradients of electron density will be given here. Attention is drawn, however, to a possible explanation of the sidereal time variation of the dispersion effects. It was noted in part I that scintillations are frequently associated with dispersion before 0900 hr sidereal time but that the incidence is low from this time until 1600 hr when observations cease. Figure 16 shows the track of the line of sight to Casseopeia A across the 200, 400, and 600 km levels. Each track has been divided up into 2-hr intervals of sidereal time. The figure also shows the 70°, 75°, and 80° isoclines (lines of constant magnetic dip). It is obvious from the figure that an isocline corresponding to a dip of 77° would cross the $h=600$ km track at about 0900 and 1600 hr sidereal time, whereas the 75° isocline crosses the $h=400$ km track at these times. The isocline corresponding to a dip in the vicinity of 75° may therefore form the northern boundary of the region with horizontal gradients of electron density suitable for the production of dispersion.

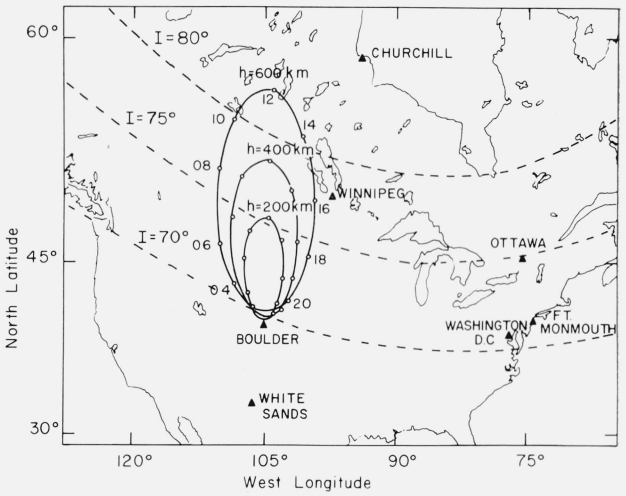

FIGURE 16. *This shows the track of the line-of-sight from Boulder to Casseopeia A across the 200, 400, and 600 km levels (full lines).*

Each of the tracks have been divided up into 2-hr intervals of sidereal time. The broken lines represent the 70, 75, and 80° isoclines and the places marked are the location of ionosondes.

8. Conclusions

The focusing action of large scale elongated ionospheric irregularities has been considered for the general case where the azimuth of the radio source and that of the short dimension of the ionospheric irregularity may both be different from that of the interferometer baseline. The expressions developed appear to explain the main features of the broadband scintillations reported in part I, namely, (a) their broad bandwidth, (b) their position shift patterns and (c) their association with spread-*F*. To reconcile the theory with the statistical information concerning position shifts it was found necessary to postulate an irregularity movement towards an azimuth of 120°. This corresponds to movement along the isoclines with the long dimension of the irregularities in the magnetic north-south direction. The results do not permit differentiation between a horizontal irregularity model and a field-alined irregularity model.

Because of a lack of knowledge of the direction of motion of individual scintillations it is not possible to find directly the range, width, or speed of the irregularities.

It is with pleasure that the author acknowledges the facilities afforded him by the High Altitude Observatory to carry out the work reported here while on sabbatical leave from the University of Queensland. In particular, he would like to thank Dr. James W. Warwick of the Observatory staff who suggested the investigation and maintained a very active interest in it.

Miss Adelle Wightman programmed the computations reported in section 4.

The research reported here was sponsored, in part, by the Air Force Cambridge Research Laboratories.

9. References

Bowman, G. G. (1959), Further studies of "spread-*F*" at Brisbane–I, Planetary Space Sci. **2,** 133–149.

Dearden, E. W. (1962), An investigation of echoes observed from Brisbane, Sci. Rept. Phys. Dept. University of Queensland, No. 13, 1–41.

Knecht, R. W., and S. Russell (1962), Pulsed radio soundings of the topside of the ionosphere in the presence of spread-*F*, J. Geophys. Res. **67,** 1178–1182.

Longhurst, R. S. (1957), Geometrical and Physical Optics (Longmans, Green and Co., London, England).

Peterson, A. M., O. G. Villard, Jr., R. L. Leadabrand, and P. B. Gallagher (1955), Regularly-observable aspect-sensitive radio reflections from ionization aligned with the earth's magnetic field and located within the ionospheric layers at middle latitudes, J. Geophys. Res. **60,** No. 4, 497–512.

Singleton, D. G. (1964), Broadband radio-star scintillations, Part I. Observations, Radio Sci. J. Res. NBS/USNC–URSI **68D,** No. 8, 867–879.

Warwick, J. W. (1964), Radio-star scintillations from ionospheric waves, Radio Sci. J. Res. NBS/USNC-URSI **68D,** No. 2, 179–188,

Wild, J. P., and J. A. Roberts (1956), The spectrum of radio-star scintillations and the nature of inequalities in the ionosphere, J. Atmospheric Terrest. Phys. **8,** 55–75.

(Paper 68D10–409)